Interplay between strong correlations and magnetic field in the symmetric periodic Anderson model

Debabrata Parihari* and N. S. Vidhyadhiraja†
Theoretical Sciences Unit, Jawaharlal Nehru Centre for Advanced Scientific Research, Jakkur, Bangalore 560064, India

David E. Logan‡
Physical and Theoretical Chemistry Laboratory, Department of Chemistry, Oxford University, South Parks Road, Oxford OX1 3QZ, United Kingdom

(Received 30 April 2008; revised manuscript received 30 June 2008; published 28 July 2008)

Magnetic-field effects in Kondo insulators are studied theoretically, using a local-moment approach to the periodic Anderson model within the framework of dynamical mean-field theory. Our main focus is on field-induced changes in single-particle dynamics and the associated hybridization gap in the density of states. Particular emphasis is given to the strongly correlated regime, where the dynamics is found to exhibit universal scaling in terms of a field-dependent low-energy coherence scale. Although the bare applied field is globally uniform, the effective fields experienced by the conduction electrons and the f electrons differ because of correlation effects. A continuous insulator-metal transition is found to occur on increasing the applied field, closure of the hybridization gap reflecting competition between Zeeman splitting, and screening of the f-electron local moments. For intermediate interaction strengths, the hybridization gap depends nonlinearly on the applied field, while in strong coupling its field dependence is found to be linear. For the classic Kondo insulator YbB_{12}, good agreement is found upon direct comparison of the field evolution of the experimental transport gap with the theoretical hybridization gap in the density of states.

DOI: 10.1103/PhysRevB.78.035128 PACS number(s): 71.27.+a, 71.28.+d, 71.30.+h, 75.20.Hr

I. INTRODUCTION

Kondo insulator materials such as SmB_6, YbB_{12}, and $Ce_3Bi_4Pt_3$ have been of sustained interest to experimentalists and theorists for several decades.[1–7] Interest in these system stems from their unusual properties, such as the small hybridization gap (of a few meV) and mixed valence, as well as the transition to metallic behavior with doping,[8] application of pressure,[9] and magnetic field.[10] The underlying qualitative origin of such rich behavior is the strong electronic correlation arising due to the localized and narrow f orbitals of the rare-earth atoms, which hybridize weakly with broad, essentially noninteracting conduction bands.

A quantitative understanding of the dynamics and transport properties of these materials has not however been easy to achieve. A principal stumbling block in this regard has been the theoretical treatment of localized and itinerant fermionic degrees of freedom on a comparable footing. Much progress has been made in recent years with the advent of dynamical mean-field theory (DMFT),[11–14] within which generic lattice-fermion models such as the Hubbard or the periodic Anderson model have found approximate solutions, and quantitative agreement with experiments has also been obtained.[11,15] Within DMFT,[11–14] a lattice-fermion model is mapped onto an effective single-site-correlated impurity which hybridizes with a self-consistent conduction-electron bath. Thus, various techniques such as the numerical renormalization group, exact diagonalization, diagrammatic perturbation theory-based approaches, quantum Monte Carlo, and many others that were, in the past, developed to handle the many-body single-impurity problem, have now been adapted and modified for use within the DMFT framework.[11–14] One such recent technique is the local-moment approach (LMA),[15–22] which has been shown to be powerful not only in the context of single-impurity systems[16–19] but also for lattice-based heavy fermion systems[15,20–22] when used in conjunction with DMFT. In this paper, we employ the LMA to understand the interplay between electronic correlations and an external magnetic field in Kondo insulator materials.

The generic model used to study Kondo insulator materials is the periodic Anderson model (PAM), which consists in physical terms of a correlated f level in each unit cell hybridizing locally with a noninteracting conduction band. Magnetic-field effects in these systems have been studied theoretically through the inclusion of a Zeeman term in the PAM.[23,24] The observed insulator-metal transition[10] has also been reproduced qualitatively in theoretical calculations.[23] However, a detailed understanding of the changes in single-particle dynamics and the associated hybridization gap on the whole has been lacking, and a quantitative description of the experimentally observed field-induced behavior has not been achieved. We seek to bridge these gaps in this paper by studying the PAM with a Zeeman term using LMA+DMFT and with particular emphasis on the strongly correlated (or strong-coupling) regime. Our primary focus is on the field-induced changes in the single-particle dynamics and the associated hybridization gap in the density of states.

The outline of the paper is as follows: We begin in Sec. II with a brief description of the model (PAM), the DMFT framework, and the LMA technique for the PAM in the presence of a magnetic field. In Sec. III we present our theoretical results and their analysis. We also make comparison between theory and experiments on the classic Kondo insulator material YbB_{12}. Brief conclusions are given in Sec. IV.

II. MODEL AND FORMALISM

The Hamiltonian for the PAM is given in standard notation by

$$H = -\sum_{\langle ij\rangle,\sigma} t_{ij} c_{i\sigma}^{\dagger} c_{j\sigma} + \sum_{i\sigma} \left(\epsilon_f + \frac{U}{2} f_{i-\sigma}^{\dagger} f_{i-\sigma} \right) f_{i\sigma}^{\dagger} f_{i\sigma} + V \sum_{i\sigma} (f_{i\sigma}^{\dagger} c_{i\sigma} + \text{H.c.}) + \epsilon_c \sum_{i\sigma} c_{i\sigma}^{\dagger} c_{i\sigma}, \quad (1)$$

where the first term describes the kinetic energy of the noninteracting conduction (c) band due to nearest-neighbor hopping t_{ij}. The second term refers to the f levels with site energies ϵ_f and on-site repulsion U, while the third term describes the c/f hybridization via the local matrix element V. The final term represents the c-electron orbital energy. Within DMFT,[11–14] which is exact in the limit of infinite dimensions, the hopping term is scaled as $t_{ij} \propto t_* / \sqrt{Z_c}$, with coordination number $Z_c \to \infty$. In this paper we consider mainly the hypercubic lattice, for which the noninteracting density of states is a Gaussian,[11] $[\rho_0(\epsilon) = \exp(-\epsilon^2/t_*^2)/\sqrt{\pi} t_*]$. We also consider specifically the (particle-hole) symmetric PAM, which is the traditional limit employed to study Kondo insulators.[11,15,22–29] For the symmetric PAM the conduction band is located symmetrically about the Fermi level (i.e., $\epsilon_c = 0$), while $\epsilon_f = -U/2$. This corresponds to half filling of the f and c levels, i.e., $n_f = \Sigma_\sigma \langle f_{i\sigma}^{\dagger} f_{i\sigma} \rangle = 1$ and $n_c = \Sigma_\sigma \langle c_{i\sigma}^{\dagger} c_{i\sigma} \rangle = 1$ for all U. In this case the system is an insulator for all interaction strengths U (in the absence of a magnetic field), with a corresponding gap in the single-particle spectra. The symmetric PAM in the absence of a magnetic field has been studied quite comprehensively within the DMFT framework; see, e.g., Refs. 11, 13, 15, 22, and 25–27.

Within DMFT, the lattice-fermion model maps onto an effective correlated single-site impurity hybridizing self-consistently with a conduction-electron bath.[11–14] The self-energy is thus spatially local, i.e., momentum independent. Thus, the problem is simplified to a great extent. Nevertheless, the problem remains nontrivial because the impurity model is as yet unsolved for an arbitrary hybridization. As mentioned in Sec. I, the local-moment approach[16] has been successful in describing the single-impurity Anderson model[16–19] as well as in understanding the PAM within DMFT.[15,20,21] Here we extend the approach to encompass finite magnetic fields in the symmetric PAM, enabling study of magnetic-field effects in Kondo insulators.

The local-moment approach begins with the symmetry broken mean-field state (unrestricted Hartree-Fock, UHF). Dynamical self-energy effects are then built in through the inclusion of transverse spin fluctuations for each of the symmetry broken states. The most important idea underlying the LMA at $T=0$ is that of symmetry restoration:[16,17,22] self-consistent restoration of the broken symmetry inherent at pure mean-field level, arising in physical terms via dynamical tunneling between the locally degenerate mean-field states and in consequence ensuring correct recovery of the local Fermi-liquid behavior that reflects adiabatic continuity in U to the noninteracting limit. The reader is referred to our earlier papers[15,22] for full details of the formalism and implementation of the zero-field LMA for the PAM.

In the presence of a global magnetic field, the degeneracy between the mean-field solutions[16] (labeled as A and B, corresponding to $+|\mu|$ and $-|\mu|$) found at the mean-field level is lifted, and only one solution as determined by $\text{sgn}(h)$ remains.[18] Here, we consider explicitly $h>0$ for which only the "A" solution survives. For $h \neq 0$ the bare electronic energy levels, ϵ_α for $\alpha = c$ and f, are of course split via the Zeeman effect. The modified energy levels are given by $\epsilon_{\alpha\sigma} = \epsilon_\alpha - \sigma h_\alpha$, with $h_\alpha = \frac{1}{2} g_\alpha \mu_B H$ (and $\sigma = \pm$ for $\uparrow/\downarrow$ spins), where μ_B is the Bohr magneton, g_α is the Landé g factor, and B is the magnetic field. Although $g_f \neq g_c$ in general, for simplicity we set $g_f = g_c = g$; i.e., we consider the application of a uniform magnetic field $h \equiv h_c = h_f$ to both c and f levels. The local (site-diagonal) Green's functions for the c and f levels may be expressed using the Feenberg renormalized perturbation theory[30,31] as

$$G_{A\sigma}^{c}(\omega;h) = \left\{ \omega^{+} + \sigma h - \frac{V^2}{\omega^{+} + \sigma h - \tilde{\Sigma}_{fA\sigma}(\omega;h)} - S_{A\sigma}[G_{A\sigma}^{c}(\omega;h)] \right\}^{-1}, \quad (2)$$

$$G_{A\sigma}^{f}(\omega;h) = \left\{ \omega^{+} + \sigma h - \tilde{\Sigma}_{fA\sigma}(\omega;h) - \frac{V^2}{\omega^{+} + \sigma h - S_{A\sigma}[G_{A\sigma}^{c}(\omega;h)]} \right\}^{-1}, \quad (3)$$

where $\omega^{+} = \omega + i\,\text{sgn}(\omega) 0^{+}$. Here $S_{A\sigma}$ is the Feenberg self-energy, a functional solely of $G_{A\sigma}^{c}$, given by

$$S_{A\sigma}(\omega;h) = \gamma_{A\sigma}(\omega;h) - \frac{1}{H[\gamma_{A\sigma}(\omega;h)]}, \quad (4)$$

with

$$\gamma_{A\sigma}(\omega;h) = \omega^{+} + \sigma h - \frac{V^2}{\omega^{+} + \sigma h - \tilde{\Sigma}_{fA\sigma}(\omega;h)}, \quad (5)$$

and the Hilbert transform $H[z]$ defined as

$$H[z] = \int_{-\infty}^{\infty} \frac{\rho_0(\epsilon) d\epsilon}{z - \epsilon} \quad (6)$$

such that $G_{A\sigma}^{c}(\omega;h) = H[\gamma_{A\sigma}]$.

Dropping the subscript A for clarity, the spin-summed Green's functions are denoted by $G^{\alpha}(\omega;h) = \frac{1}{2}\Sigma_\sigma G_\sigma^{\alpha}(\omega;h)$ $(\alpha = c, f)$, with corresponding spectral functions $D^{\alpha}(\omega;h) = -\frac{1}{\pi}\text{sgn}(\omega)\text{Im}\, G^{\alpha}(\omega;h)$. Within the LMA the f-electron self-energies $\tilde{\Sigma}_{f\sigma}(\omega;h)$ are familiarly separated into a static mean-field contribution plus a dynamical part $\Sigma_{f\sigma}(\omega;h)$,[15,16,22]

$$\tilde{\Sigma}_{f\sigma}(\omega;h) = -\frac{\sigma}{2} U |\bar{\mu}(h)| + \Sigma_{f\sigma}(\omega;h), \quad (7)$$

where $|\bar{\mu}(h)|$ is the UHF local moment. We approximate the dynamical part of the self-energy by the usual nonperturba-

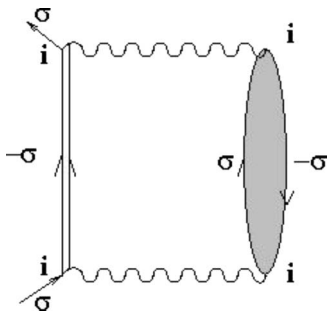

FIG. 1. Principal contribution to the LMA $\{\Sigma_{f\sigma}(\omega)\}$. The wavy lines denote U. See text for details.

tive class of diagrams retained in practice by the LMA (as shown in Fig. 1), which may be expressed mathematically at zero temperature[15,16,22] as

$$\Sigma_{f\sigma}(\omega;h) = U^2 \int_{-\infty}^{\infty} \frac{d\omega_1}{2\pi i} \mathcal{G}_{-\sigma}(\omega-\omega_1;h)\Pi^{-\sigma\sigma}(\omega_1;h). \quad (8)$$

Here the host/medium Green's function $\mathcal{G}_\sigma$ (denoted by the double-lined propagator in Fig. 1) is defined by

$$\mathcal{G}_\sigma(\omega;h)^{-1} = G^f_\sigma(\omega;h)^{-1} + \Sigma_{f\sigma}(\omega;h). \quad (9)$$

$\Pi^{-\sigma\sigma}(\omega;h)$ denotes the transverse spin-polarization propagator (shown shaded in Fig. 1), which in the random-phase approximation employed is expressed as $\Pi^{+-}={}^0\Pi^{+-}/(1-U{}^0\Pi^{+-})$. The bare polarization propagator ${}^0\Pi^{+-}(\omega;h)$ is expressed in terms of mean-field propagators[15,22] $\{g^\alpha_\sigma(\omega;h)\}$ (in which only the static Fock contribution to the self-energies occurs).

For $h=0$ the symmetry restoration (SR) condition for the symmetric PAM is given by[15,22] $\tilde{\Sigma}_{f\sigma}(\omega=0;h=0)=0$ [independent of spin σ, since by particle-hole symmetry $\tilde{\Sigma}_{f\sigma}(\omega;h)=-\tilde{\Sigma}_{f-\sigma}(-\omega;h)$], i.e., by

$$\Sigma_{f\uparrow}(\omega=0;h=0) = U|\bar{\mu}|/2. \quad (10)$$

Satisfaction of the SR condition ensures adiabatic continuity (in U) to the noninteracting limit[15,22] of the hybridization-gap insulator (the system being in that sense a generalized Fermi liquid[15,22]). As expected the system remains insulating, with a gap in the single-particle spectra, for all interactions $U \geq 0$.

The practical implementation of the above procedure is carried out as follows,[15,21,22] in which the numerical procedure is simplified by keeping $x=\frac{1}{2}U|\mu|$ fixed while varying U to satisfy the symmetry restoration condition. We begin with an $h=0$ calculation for a given x. (i) The mean-field Green's functions $g^\alpha_\sigma(\omega;h)$ are obtained from Eqs. (2)–(7) by retaining only the static part of the self-energy. (ii) These Green's functions are then used to construct the bare polarization bubble ${}^0\Pi^{+-}$. (iii) The DMFT iterative procedure starts with a specific dynamical self-energy, obtained either as a guess or from the previous iteration, which is substituted into Eqs. (2)–(7) to get the c and f Green's functions. (iv) The host/medium Green's function $\mathcal{G}_\sigma(\omega;h)$ is obtained through Eq. (9). (v) The transverse spin-polarization propagator Π^{+-} is computed for a given U and along with $\mathcal{G}_\sigma(\omega;h)$, substituted in Eq. (8) to determine the $\omega=0$ self-energy for a given U. (vi) The SR condition [Eq. (10)] is checked, and if found not to be satisfied, U is varied and step (v) is repeated until the SR condition is satisfied. (vii) Upon restoration of the broken spin symmetry, the corresponding U is obtained and Eq. (8) may then be used to get the full dynamical self-energy at all frequencies. (viii) The new self-energy is fed back into the first step of the DMFT procedure [step (iii)] and the iterations are continued until full self-consistency is achieved. For finite fields the same procedure is adopted except that SR is no longer imposed[18] (the U found from SR at $h=0$ is naturally used for all $h>0$).

III. RESULTS AND DISCUSSION

Before discussing the interplay between interactions and magnetic fields in the symmetric PAM, we consider briefly two limiting cases: (i) the noninteracting limit, $U=0$, with $h\neq 0$; and (ii) the interacting problem $U>0$ in the absence of a field. In the former case, the noninteracting c spectrum for spin σ is given by

$$d^c_{0\sigma}(\omega;h) = \rho_0\left(\omega+\sigma h - \frac{V^2}{\omega+\sigma h}\right).$$

The spectral band edges are given by

$$\omega+\sigma h - \frac{V^2}{\omega+\sigma h} = \pm W, \quad (11)$$

where $2W$ is the full bandwidth of the noninteracting density of states $\rho_0(\omega)$. It is easy to see from this that for $h=0$ there is a hybridization gap at the Fermi level [denoted by $\Delta_0(0)$], which decreases with increasing field h and eventually closes at a field value that is half of the zero-field spectral gap, i.e.,

$$\Delta_0(h) = \Delta_0(0) - 2h. \quad (12)$$

Thus in the noninteracting limit, the application of a magnetic field leads to an insulator-metal transition simply because of the rigid crossing of the up- and down-spin bands. We add here that the noninteracting Gaussian density of states characteristic of the hypercubic lattice (as considered explicitly below) is of course unbounded and as such does not possess "hard" band edges. The field-induced insulator-metal transition in this case is thus strictly a crossover, although in practice the transition is "sharp," as one would expect (discussed later, see, e.g., Fig. 5).

In the second limit, of finite interactions but zero field, the ground state remains gapped for all interaction strengths,[22] the hybridization gap Δ decreasing continuously with increasing U from its noninteracting limit $\Delta_0(0)$. In the strong-coupling, Kondo lattice regime of the model, universal scaling occurs[15,22,26,28,29] in terms of an exponentially small low-energy scale $\omega_L=ZV^2/t_*(\equiv\frac{1}{2}\Delta)$. Z is the quasiparticle weight or mass-renormalization factor, given by $Z=[1-\partial\Sigma_{f\sigma}(\omega)/\partial\omega|_{\omega=0}]^{-1}$. Green's functions and their associated spectra depend solely on $\tilde{\omega}=\omega/\omega_L$ in the universal scaling regime.[15,22] Representative results for the zero-field density of states are shown in Fig. 2, where the main panels show the

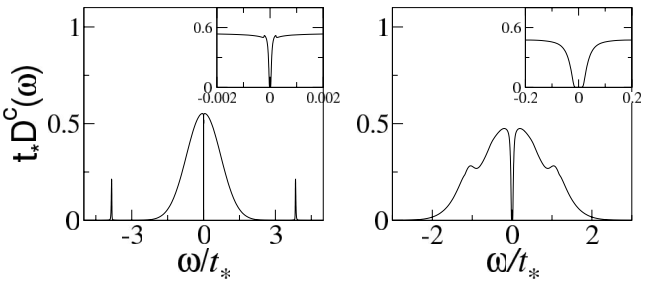

FIG. 2. LMA conduction-electron spectra for $h=0$ in strong coupling (left panel, $U/t_*=7.1$) and weaker coupling (right panel, $U/t_*=1.2$), with $V^2=0.2t_*^2$. The insets show the low-frequency region of the respective main panels.

conduction-band density of states, $t_*D^c(\omega)$ (solid lines), as a function of frequency, ω/t_*. The right panels represent intermediate coupling ($U/t_*=1.2$), while the left panels are for strong coupling ($U/t_*=7.1$). The insets show a closeup of the low-frequency spectra where the hybridization gap at the Fermi level ($\omega=0$) is evident at both weak and strong couplings.

Now we consider both interactions and the field. In the strong-coupling regime, parallel to the $h=0$ limit, we expect universality to persist in terms of a field-dependent low-energy scale, $\omega_L \equiv \omega_L(h)$. To derive explicitly the universal scaling form in the limit of low frequencies (i.e., close to the Fermi level), we perform a simple low-frequency "quasiparticle expansion" of the self-energy, retaining only its real part ($\Sigma^R_{f\sigma}$) to leading order in ω; i.e.,

$$\Sigma^R_{f\sigma}(\omega;h) = \Sigma^R_{f\sigma}(0;h) - \left[\frac{1}{Z(h)} - 1\right]\omega, \tag{13}$$

where $Z(h)=[1-\partial\Sigma^R_{f\sigma}(\omega;h)/\partial\omega|_{\omega=0}]^{-1}$ is the field-dependent quasiparticle weight [independent of σ since $\Sigma^R_{f\sigma}(\omega;h) = -\Sigma^R_{f-\sigma}(-\omega;h)$ by particle-hole symmetry].

Substituting Eq. (13) into Eqs. (2)–(7), we find that the associated spectral functions are just renormalized versions of their noninteracting counterparts, being given by

$$D^c_\sigma(\omega;h) \overset{\omega\to 0}{\to} \rho_0\left(-\frac{1}{\tilde{\omega}+\sigma h_{\rm eff}}\right), \tag{14}$$

$$D^f_\sigma(\omega;h) \overset{\omega\to 0}{\to} \frac{t_*^2}{V^2}\frac{1}{(\tilde{\omega}+\sigma h_{\rm eff})^2}D^c_\sigma(\omega;h), \tag{15}$$

where $\tilde{\omega}=\omega/\omega_L(h)$, and the low-energy scale $\omega_L(h) = Z(h)V^2/t_*$ is thus defined (in direct parallel to the $h=0$ limit). In obtaining Eqs. (14) and (15), we have explicitly considered the strong-coupling scaling regime, of finite $\tilde{\omega} = \omega/\omega_L(h)$ and $h/\omega_L(h)$ in the formal limit where the low-energy scale $\omega_L \to 0$ (so that "bare" factors of $\omega \equiv \tilde{\omega}\omega_L$ or h are thus neglected). $h_{\rm eff}$ in Eqs. (14) and (15) is given by

$$h_{\rm eff} = [h - \sigma\tilde{\Sigma}^R_{f\sigma}(0;h)]\frac{t_*}{V^2} \tag{16}$$

(being independent of σ, by symmetry), or equivalently, using the symmetry restoration condition $\tilde{\Sigma}^R_{f\sigma}(0;0)=0$, by

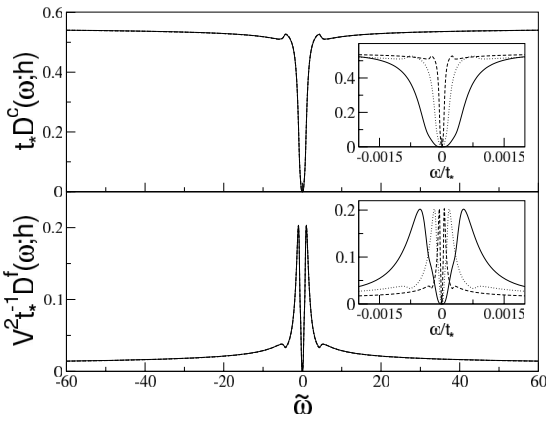

FIG. 3. LMA spectra for the c electrons [top panel, $t_*D^c(\omega;h)$] and f electrons [bottom panel, $V^2t_*^{-1}D^f(\omega;h)$] for three parameter sets, each corresponding to a fixed $h_{\rm eff}=0.27$: $Ut_*/V^2=35$, $h/t_* = 2.4\times10^{-5}$ (dashed), $Ut_*/V^2=30$, $h/t_*=7.4\times10^{-5}$ (dotted), and $Ut_*/V^2=25$, $h/t_*=2.3\times10^{-4}$ (solid). The insets show the spectra vs the bare frequency, ω/t_*. Main panel: the same spectra plotted vs $\tilde{\omega}=\omega/\omega_L(h)$ collapse to a common scaling form.

$$h_{\rm eff} = \{h + \sigma[\tilde{\Sigma}^R_{f\sigma}(0;0) - \tilde{\Sigma}^R_{f\sigma}(0;h)]\}\frac{t_*}{V^2}. \tag{17}$$

In physical terms, $h_{\rm eff}$ represents a dimensionless effective field, and its primary field dependence arises from that of the interaction self-energy [the bare factor of h in Eq. (16) or (17) can of course be dropped in the strict scaling limit, although we retain it for clarity]. In fact a leading-order Taylor expansion of Eq. (16) or (17) gives $h_{\rm eff}=c\tilde{h}$, where $\tilde{h} = h/\omega_L(0)$ is the field rescaled in terms of the $h=0$ low-energy scale $\omega_L(h=0)=Z(0)V^2/t_*$, and $c=Z(0)/\tilde{Z}$ [$\sim\mathcal{O}(1)$], with $\tilde{Z}=\{1-\sigma[\partial\tilde{\Sigma}^R_{f\sigma}(0;h)/\partial h]_{h=0}\}^{-1}$ thus defined. From this simple consideration, we anticipate that $h_{\rm eff}$ is just a rescaled version of the bare magnetic field itself and is on the order of $\tilde{h}=h/\omega_L(0)$ (as confirmed explicitly later, see, e.g., Fig. 5).

Equations (14) and (15) show that in strong coupling, the spectra $D^c(\omega;h)$ and $V^2D^f(\omega;h)$ should be universal functions of $\tilde{\omega}=\omega/\omega_L(h)$ for a fixed $h_{\rm eff}$. Thus, if distinct sets of model parameters in the strong-coupling regime correspond to the same $h_{\rm eff}$, the spectra D^c and V^2D^f should collapse to the same scaling form as a function of $\tilde{\omega}$, *independently* of the bare parameters U/t_* and V/t_*. That this is so is illustrated in Fig. 3, where the top panel shows the full LMA c-electron spectra t_*D^c for the hypercubic lattice and the bottom panel shows the corresponding f-electron spectra $(V^2/t_*)D^f$. Three sets of spectra are shown, with parameters $Ut_*/V^2=35$ and $h/t_*=2.4\times10^{-5}$ (dashed), $Ut_*/V^2=30$ and $h/t_*=7.4\times10^{-5}$ (dotted), and $Ut_*/V^2=25$ and $h/t_*=2.3\times10^{-4}$ (solid). In all cases, $h_{\rm eff}$ (=0.27) is the same. The insets of the figure show that the spectra as a function of the bare frequency ω/t_* are distinct. However when plotted vs $\tilde{\omega}$ (as shown in the main panels), they are indeed seen to collapse to a single universal form.

The quasiparticle forms in Eqs. (14) and (15) embody local Fermi-liquid behavior and adiabatic continuity to the noninteracting limit. They give explicitly the leading low-

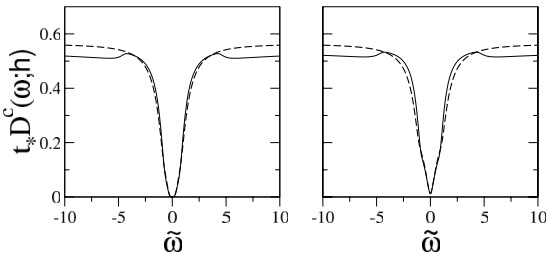

FIG. 4. Full LMA c-electron scaling spectra (solid lines) are compared to the limiting quasiparticle form, Eq. (14) (dashed lines). The left panel shows the scaling spectra for $h_{\rm eff}=0.27$ (where the system is an insulator) and the right panel that for $h_{\rm eff}=0.51$ (metallic).

frequency asymptotic behavior of the scaling spectra that must be satisfied by any "full" theory. Direct comparison between the quasiparticle forms and the full LMA scaling spectra is shown in Fig. 4 for the c-electron spectra and for two values of the effective field $h_{\rm eff}$ (one corresponding to a case where the system remains insulating and the other for a higher field where the system is metallic, as discussed below). It is indeed clear from the figure that the LMA correctly recovers the limiting quasiparticle form in the vicinity of the Fermi level. In physical terms it is also worth noting that the low-frequency quasiparticle spectra are essentially those for the noninteracting limit but with the local fields for f and c electrons replaced by $(V^2/t_*)h_{\rm eff}$ and zero, respectively. Hence, although the bare applied field is globally uniform, the effective local fields experienced by the c and f electrons are different because of correlation effects.

We turn now to the transition with increasing field from an insulating state characterized by a spectral gap straddling the Fermi level to a metal with a finite density of states at $\omega=0$. Equations (14) and (15) may be used to obtain an estimate of the spectral band edges in strong coupling and hence the gap as a function of the field. The band edges are given by

$$\frac{1}{\tilde{\omega}+\sigma h_{\rm eff}} = \pm W/t_*, \tag{18}$$

with $2W$ as the bandwidth of the noninteracting spectrum. From this the field-dependent gap in $D^c(\omega;h)$ or $D^f(\omega;h)$ follows as

$$\Delta(h) = 2\left(1 - h_{\rm eff}\frac{W}{t_*}\right)\frac{Z(h)V^2}{W}. \tag{19}$$

This in turn implies an insulator-to-metal transition at a critical effective field $h_{{\rm eff},c}$ that is on the order of unity $(\sim t_*/W)$. The main panel in Fig. 5 shows the variation in the full LMA density of states at the Fermi level, $D^c(\omega=0;h)$ (calculated explicitly for $U/t_*=6.1$, $V^2/t_*^2=0.2$), as a function of $h_{\rm eff}$ on a logarithmic scale. Although the calculations are for a hypercubic lattice, with a strictly soft gap in its zero-field spectrum, the insulator-metal transition is seen in practice to be sharp, occurring at a critical $h_{{\rm eff},c}\simeq 0.36$ that is indeed on the order of unity [we identify the critical field in practice from $t_* D^c(0;h_c)\sim 10^{-3}$]. On further increase in the

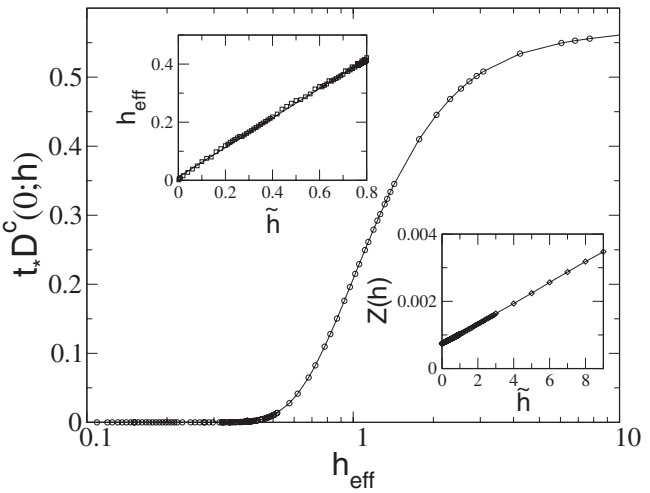

FIG. 5. c-band spectrum at the Fermi level $D^c(0;h)$ in the strong-coupling, universal regime as a function of $h_{\rm eff}$, showing a continuous insulator-metal transition at $h_{{\rm eff},c}\simeq 0.36$. Top inset: linear dependence of the effective field $h_{\rm eff}$ on $\tilde{h}=h/\omega_L(0)$ $[\omega_L(0)=Z(0)V^2/t_*]$. Bottom inset: linear increase in the quasiparticle weight $Z(h)$ with increasing $\tilde{h}$.

field, $D^c(0;h)$ is seen from the figure to rise continuously, toward the high-field value of $1/\sqrt{\pi}t_*$ which is just the noninteracting density-of-states (dos) value at the Fermi level.

The top inset of Fig. 5 shows the dependence of the effective field $h_{\rm eff}$ [Eqs. (16) and (17)] on the scaled external field $\tilde{h}=h/\omega_L(0)$ [with $\omega_L(0)=Z(0)V^2/t_*$]. $h_{\rm eff}$ is seen to be linear in $\tilde{h}$ (whose behavior extends over a wide $\tilde{h}$ interval) and, as anticipated above, is on the same order as it: $h_{\rm eff}\simeq\tilde{h}/2$, as evident from the figure. The lower inset to the figure also shows the $\tilde{h}$ dependence of the quasiparticle weight $Z(h)$. It too is seen to increase linearly with field, implying a lowering of effective mass with an increase in field, and whose behavior is consistent with a similar finding for the single-impurity Anderson model.[18]

The field dependence of the full density of states is illustrated in Fig. 6, where we plot the (universal, strong-coupling) conduction-band density of states $D^c(\omega;h)$ as a

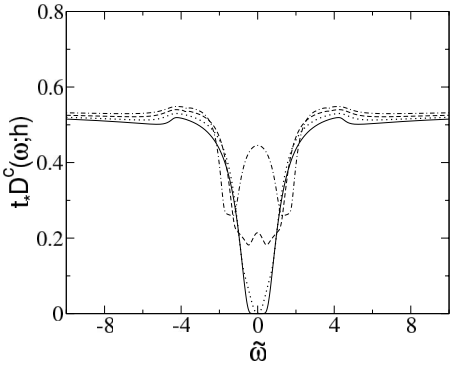

FIG. 6. Universal c-electron spectra from the LMA are shown as a function of $\tilde{\omega}=\omega/\omega_L$ for various fields: $h_{\rm eff}=0$ (solid), $h_{\rm eff}=0.38$ (dotted), $h_{\rm eff}=1$ (dashed), and $h_{\rm eff}=5$ (dot dashed). The closure of the insulating gap with increasing field is evident.

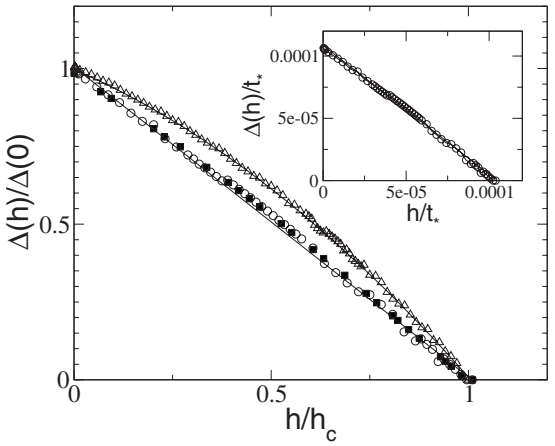

FIG. 7. The field-dependent spectral gap scaled by the zero-field gap, $\Delta(h)/\Delta(0)$, vs h/h_c for $U/t_*=1.2$, $V^2/t_*^2=0.2$ (triangles), $U/t_*=5.1$, $V^2/t_*^2=0.2$ (squares), and $U/t_*=6.1$, $V^2/t_*^2=0.2$ (circles). (The lines are best fits to the points.) Inset: the gap in units of t_* vs the bare field h/t_*.

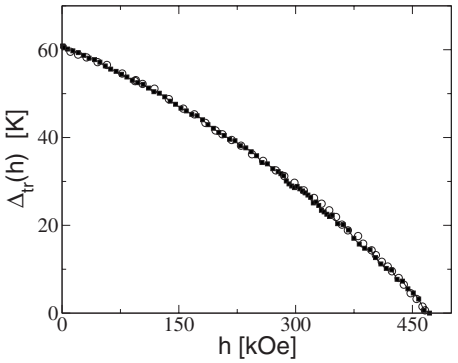

FIG. 8. Comparison of the experimental (Ref. 10) transport gap in YbB_{12} (open circles) to the theoretical gap (filled squares), obtained as discussed in text. The theory is seen to describe well the functional form of the transport gap.

function of the $\tilde{\omega}$ for various $h_{\rm eff}$. The solid curve $h_{\rm eff}=0$ represents the insulating ground state, while the dotted curve is for $h_{\rm eff}=0.38$, which is just above the insulator-metal transition, so the gap has closed. The remaining curves are for $h_{\rm eff}=1$ and $h_{\rm eff}=5$, showing metallic densities of states characterized by a finite spectral density $D^c(0;h)$ at the Fermi level.

In the noninteracting limit, $U=0$, the spectral gap closes linearly with the applied field as in Eq. (12), and the essential mechanism for the insulator-metal transition is obvious: Zeeman splitting moves the up- and down-spin bands rigidly, resulting in their crossing at a critical field, $h_{c0}/\Delta_0(0)=\frac{1}{2}$. This simple picture is naturally modified in the presence of correlations, $U>0$, where two essentially competing effects are operative. First, the tendency of the system to lower its energy by uniform ("ferromagnetic") spin polarization of the c and f electrons, i.e., the Zeeman effect, which alone operates in the noninteracting limit. However for $h=0$ in the presence of interactions, lattice-coherent Kondo singlet formation occurs, driven by local *anti*ferromagnetic spin correlations between the c and f electrons. In the presence of both interactions *and* a field, Zeeman splitting thus in effect competes with local-moment screening. The field dependence of the spectral gap is not *a priori* obvious.

LMA results for the spectral gap are shown in Fig. 7, where the field-dependent gap scaled by the zero-field gap, $\Delta(h)/\Delta(0)$, is plotted vs h/h_c for various interaction strengths. For intermediate coupling [$U/t_*=1.2$, $V^2/t_*^2=0.2$ (triangles)], the gap is seen to close nonlinearly in the field and is best fitted by a quadratic form. In the strong-coupling regime by contrast (squares, $U/t_*=5.1$, $V^2/t_*^2=0.2$ and circles, $U/t_*=6.1$, $V^2/t_*^2=0.2$), the linear behavior $\Delta(h)=\Delta(0)(1-h/h_c)$ is obtained, similar to that in the noninteracting limit. In this case however, when $\Delta(h)$ is plotted directly vs the bare field h/t_* as shown in the inset of Fig. 7, the functional form obtained is $\Delta(h)=\Delta(0)-h$, which shows that the field h_c required to close the gap in strong coupling satisfies $h_c/\Delta(0)=1$, i.e., twice of that required in the noninteracting limit, where $h_{c0}/\Delta_0(0)=\frac{1}{2}$. This result is physically natural, in view of the effective competition between Zeeman splitting and local-moment screening discussed above.

Finally, we would like to make a comparison of our theoretical results to experiment. For the classic Kondo insulator YbB_{12}, the field dependence of the transport gap has been determined from low-temperature resistivity measurements[10] [the leading low-T behavior of the resistivity being $\rho(T)\propto\exp(-\Delta_{\rm tr}/T)$, with $\Delta_{\rm tr}\equiv\Delta_{\rm tr}(h)$ as the transport/activation gap]. Since the transport gap is known theoretically[15] to be proportional to the spectral gap [$\Delta(0)\simeq 2\Delta_{\rm tr}(0)$ (Ref. 15)], a comparison to experiment may be made.

In our earlier work,[15] where we compared the zero-field transport properties of YbB_{12} to theoretical results from the LMA, we concluded that YbB_{12} belongs to the intermediate-coupling regime (and as such lies outside the universal scaling regime). This is corroborated by the field dependence of the transport gap, the experimental results for which[10] are shown as open circles in Fig. 8. The dependence of $\Delta_{\rm tr}(h)$ on the field h is clearly nonlinear, whose behavior we have found above to be characteristic of the intermediate-coupling regime. To make comparison to experiment in this regime, certain model parameters must of course be specified, and here we choose $U/t_*=1.2$, $V^2/t_*^2=0.2$ (the essential results are quite insensitive to these particular values). The filled squares in Fig. 8 show the field dependence of the resultant theoretical spectral gap, compared directly to experiment with a simple multiplicative scaling of the x and y axes. The functional form of the theoretical gap is seen to be almost identical to that found experimentally, thus yielding good agreement between theory and experiment. Further, since the experimental $\Delta_{\rm tr}(0)\simeq 60$ K (Fig. 8), then the spectral gap $\Delta(0)\simeq 2\Delta_{\rm tr}(0)\simeq 120$ K. Moreover for the bare parameters considered, we find $\Delta(0)=0.026t_*$. This in turn yields the estimate $t_*\simeq 0.4$ eV, which is physically realistic and compatible with transfer integral values found through a band-structure calculation.[32]

IV. CONCLUSION

The interplay between electronic correlations and an externally applied magnetic field in Kondo insulators has been

considered in this paper. The symmetric periodic Anderson model, with a Zeeman term to account for the external magnetic field, has been studied within the dynamical mean-field framework using a local-moment approach. In the strong-coupling Kondo lattice regime of the model, the local c- and f-electron spectral functions are found to exhibit universal scaling, being functions solely of ω/ω_L [with $\omega_L(h) = Z(h)V^2/t_*$ the characteristic low-energy scale] for a given effective field h_{eff}. Although the externally applied field is globally uniform, the effective local fields experienced by the c and f electrons differ because of correlation effects. The zero-field spectral gap characteristic of Kondo insulators is found to close continuously, leading to a continuous insulator-metal transition at a critical applied field h_c. The field-induced closure of the insulating gap is not simply a rigid band-crossing affair but involves competition between local-moment screening (reflecting correlation effects) and Zeeman spin polarization. In the intermediate-coupling regime, the gap is found to close nonlinearly with field, while in the strong-coupling regime it closes linearly. Comparison of the theoretical gap with the transport gap measured in the intermediate-coupling material YbB_{12} yields good agreement, providing support to the scenario presented for the field-induced gap closure.

ACKNOWLEDGMENTS

The authors D.P. and N.S.V. would like to thank CSIR, India, and JNCASR, India, while D.E.L. would like to thank EPSRC-GB for supporting this research.

*dparihari@jncasr.ac.in
†Corresponding author. raja@jncasr.ac.in
‡dlogan@physchem.ox.ac.uk

[1] N. Grewe and F. Steglich, *Handbook on the Physics and Chemistry of Rare Earths*, edited by K. A. Gschneider, Jr. and L. L. Eyring (Elsevier, Amsterdam, 1991), Vol. 14.
[2] A. C. Hewson, *The Kondo Problem to Heavy Fermions* (Cambridge University Press, Cambridge, 1993).
[3] G. Aeppli and Z. Fisk, Comments Condens. Matter Phys. **16**, 155 (1992).
[4] Z. Fisk, J. L. Sarrao, S. L. Cooper, P. Nyhus, G. S. Boebinger, A. Passner, and P. C. Canfield, Physica B (Amsterdam) **223-224**, 409 (1996).
[5] T. Takabatake *et al.*, J. Magn. Magn. Mater. **177-181**, 277 (1998).
[6] L. Degiorgi, Rev. Mod. Phys. **71**, 687 (1999).
[7] Peter S. Riseborough, Adv. Phys. **49**, 257 (2000).
[8] J. F. DiTusa, K. Friemelt, E. Bucher, G. Aeppli, and A. P. Ramirez, Phys. Rev. Lett. **78**, 2831 (1997).
[9] A. Barla, J. Derr, J. P. Sanchez, B. Salce, G. Lapertot, B. P. Doyle, R. Ruffer, R. Lengsdorf, M. M. Abd-Elmeguid, and J. Flouquet, Phys. Rev. Lett. **94**, 166401 (2005).
[10] K. Sugiyama, F. Iga, M. Kasaya, T. Kasaya, and M. Date, J. Phys. Soc. Jpn. **57**, 3946 (1988).
[11] A. Georges, G. Kotliar, W. Krauth, and M. Rozenberg, Rev. Mod. Phys. **68**, 13 (1996).
[12] D. Vollhardt, in *Correlated Electron Systems*, edited by V. J. Emery (World Scientific, Singapore, 1993), Vol. 9.
[13] T. Pruschke, M. Jarrell, and J. K. Freericks, Adv. Phys. **44**, 187 (1995).
[14] F. Gebhard, *The Mott Metal-Insulator Transition*, Springer Tracts in Modern Physics Vol. 137 (Springer, Berlin, 1997).
[15] N. S. Vidhyadhiraja, V. E. Smith, D. E. Logan, and H. R. Krishnamurthy, J. Phys.: Condens. Matter **15**, 4045 (2003).
[16] D. E. Logan, M. P. Eastwood, and M. A. Tusch, J. Phys.: Condens. Matter **10**, 2673 (1998); M. T. Glossop and D. E. Logan, *ibid.* **14**, 6737 (2002); D. E. Logan and M. T. Glossop, *ibid.* **12**, 985 (2000).
[17] N. L. Dickens and D. E. Logan, J. Phys.: Condens. Matter **13**, 4505 (2001).
[18] D. E. Logan and N. L. Dickens, Europhys. Lett. **54**, 227 (2001); J. Phys.: Condens. Matter **13**, 9713 (2001).
[19] R. Bulla, M. T. Glossop, D. E. Logan, and T. Pruschke, J. Phys.: Condens. Matter **12**, 4899 (2000).
[20] N. S. Vidhyadhiraja and D. E. Logan, J. Phys.: Condens. Matter **17**, 2959 (2005).
[21] N. S. Vidhyadhiraja and D. E. Logan, Eur. Phys. J. B **39**, 313 (2004).
[22] V. E. Smith, D. E. Logan, and H. R. Krishnamurthy, Eur. Phys. J. B **32**, 49 (2003).
[23] T. Saso, J. Phys. Soc. Jpn. **66**, 1175 (1997).
[24] K. S. D. Beach, P. A. Lee, and P. Monthoux, Phys. Rev. Lett. **92**, 026401 (2004).
[25] M. Jarrell, Phys. Rev. B **51**, 7429 (1995).
[26] Y. Shimizu and O. Sakai, *Computational Physics as a New Frontier in Condensed Matter Research*, edited by H. Takayama *et al.* (The Physical Society of Japan, Tokyo, 1995); T. Pruschke, R. Bulla, and M. Jarrell, Phys. Rev. B **61**, 12799 (2000); M. Jarrell, H. Akhlaghpour, and T. Pruschke, Phys. Rev. Lett. **70**, 1670 (1993).
[27] S. J. Sun, M. F. Yang, and T. M. Hong, Phys. Rev. B **48**, 016127 (1993); E. Halvorsen and G. Czycholl, J. Phys.: Condens. Matter **8**, 1775 (1996); D. Meyer and W. Nolting, Phys. Rev. B **61**, 13465 (2000).
[28] T. Pruschke and N. Grewe, Z. Phys. B: Condens. Matter **74**, 439 (1989); T. M. Rice and K. Ueda, Phys. Rev. B **34**, 6420 (1986).
[29] P. Fazekas and B. Brandow, Phys. Scr. **36**, 809 (1987); P. Fazekas, J. Magn. Magn. Mater. **63&64**, 545 (1987).
[30] E. Feenberg, Phys. Rev. **74**, 206 (1948).
[31] E. N. Economou, *Green's Functions in Quantum Mechanics* (Springer, Berlin, 1983).
[32] T. Saso and H. Harima, J. Phys. Soc. Jpn. **72**, 1131 (2003).